myjournal manuscript No.
(will be inserted by the editor)

Simulation of typical Cox–Voronoi cells with a special regard to implementation tests

C. Gloaguen[1], **F. Fleischer**[2], **H. Schmidt**[3], **V. Schmidt**[3]

[1] France Télécom R&D TECH/LEI/MOT 92131 Issy les Moulineaux Cedex 9, France
[2] Department of Applied Information Processing and Department of Stochastics, University of Ulm, 89069 Ulm, Germany
[3] Department of Stochastics, University of Ulm, 89069 Ulm, Germany

Received: date / Revised version: date

Abstract We consider stationary Poisson line processes in the Euclidean plane and analyze properties of Voronoi tessellations induced by Poisson point processes on these lines. In particular, we describe and test an algorithm for the simulation of typical cells of such Cox–Voronoi tessellations. Using random testing, we validate our algorithm by comparing theoretical values of functionals of the zero cell to simulated values obtained by our algorithm. Finally, we analyze geometric properties of the typical Cox–Voronoi cell and compare them to properties of the typical cell of other well–known classes of tessellations, especially Poisson–Voronoi tessellations. Our results can be applied to stochastic–geometric modelling of networks in telecommunication and life sciences, for example. The lines can then represent roads in urban road systems, blood arteries or filament structures in biological tissues or cells, while the points can be locations of telecommunication equipment or vesicles, respectively.

Key words: Stochastic geometry, Random tessellation, Typical cell, Shape analysis, Network, Random software testing

AMS 2000 **subject classification**: 60D05, 90B15, 68U20

1 Introduction

The Voronoi tessellation is one of the most popular model for subdividing the Euclidean plane into convex and compact subsets. These subsets, called Voronoi cells, are polygons constructed according to the nearest neighbor

principle with respect to a set of nuclei. Applications of such tessellation models arise in numerous fields, e.g. in economics, biology, and telecommunication; see Okabe et al. [10] and the references therein.

A special, but important class of Voronoi tessellations are so–called Poisson–Voronoi tessellations (PVT), which are obtained if the nuclei are realizations of (homogeneous) Poisson point processes. The principle of homogeneity (or, in other words, stationarity) of the generating point process is often modified to suit application purposes; see e.g. Błaszczyszyn and Schott [2], Okabe et al. [10]. For example in the context of telecommunication or life sciences, one considers models where the points are no longer randomly scattered in the whole plane but are situated on lines which itself can be randomly distributed. In telecommunication the lines could represent roads in urban road systems while the points are locations of telecommunication equipment or cars; see e.g. Gloaguen et al. [4,5]. In life sciences the lines could represent blood arteries or filament structures in biologic tissues or cells; see e.g. Schütz [12] and the references therein.

In the present paper, we consider configurations of lines induced by stationary Poisson line processes and we analyze Voronoi tessellations whose nuclei form (inhomogenous) Poisson point processes on the lines. We call such a division of the plane a *Cox–Voronoi tessellation* (CVT) since its nuclei are realizations of doubly stochastic Poisson point processes, which are also called *Cox processes* by some authors. By means of CVT, the spatial structure of the underlying Cox processes can be investigated. Furthermore, in the context of telecommunication, the cells of CVT can be seen as *serving zones* of their respective nuclei.

Important properties of stationary CVT can be comprehended by their *typical cell*, which is, roughly speaking, the cell drawn uniformly out of the set of all possible cells. Using dictions of Palm theory, the typical cell can be thought of as the cell that contains the origin under the condition that the underlying Cox process has a point at the origin. We show how this Palm principle can be applied to develop an efficient algorithm for the simulation of the typical cell of CVT. Since only very few analytical formulae are known for CVT, simulation of the typical Cox–Voronoi cell is useful in order to get knowledge about first–order and second–order moments and especially about distributional properties of certain cell characteristics like the number of vertices, the area, or the perimeter. This knowledge can be applied, for example, in modelling of telecommunication networks to perform effective cost analyzes with respect to serving zones of telecommunication equipment.

The developed algorithm must of course be validated, where the validation can be seen from different viewpoints: from the perspectives of mathematical statistics and computer science, respectively. Since the output of our algorithm is random, tests designed for randomized software are applied. Over the last decades an enormous amount of literature dealing with methods for testing software in a general meaning has been published; see e.g. Binder [1] and Sneed [13]. However, the testing of software with random input or random output has been almost completely neglected. Therefore

publications concerning this topic are very scarce; see e.g. Mayer and Guderlei [7]. Hence, besides describing our algorithm, we explore random test techniques in order to ensure correctness of the algorithm.

Typically, one can distinguish between testing by using known theoretical formulae for certain characteristics and testing by comparison to already existing algorithms. We illustrate both methods, which are based on statistical significance tests. Furthermore, in the case of the typical Cox–Voronoi cell, certain scaling–invariance properties can be used to test the algorithm by comparison to itself, i.e., by comparison between different values of input parameters. This technique allows us to test also for correctness of second–order moments which was rarely done before in the context of random software testing. The tested implementation of the algorithm is included in the GeoStoch library, which is a Java–based open–library system developed by the Departments of Applied Information Processing and Stochastics of the University of Ulm. Notice that the GeoStoch system has been designed mainly for stochastic–geometric modelling and spatial statistical analysis of image date on geographic–cartographic as well as microscopic scales; see Mayer et al. [8] and http://www.geostoch.de.

Finally, we compare our simulation results for the typical Cox–Voronoi cell to results obtained by analytical formulae for the typical cell of PVT. Obviously, both models are closely related and it is interesting to see which kind of relationships exists between them or what are the differences between these two classes of tessellations.

The paper is organized as follows. Some necessary mathematical background is given in Section 2, especially the description of the Cox–Voronoi model. Section 3 is devoted to the simulation algorithm for the typical Cox–Voronoi cell. Methods for testing and validating this algorithm are discussed in Section 4, where different techniques are applied: the comparison to known analytical formulae, the comparison to other related algorithms, and the comparison to results for different values of input parameters. In Section 5, numerical results for specific values of parameter pairs are closely inspected, where it is shown how one can get results for any pair of given parameters using the displayed values. Then, in a second part of Section 5, the simulation results are compared to results obtained by analytical formulae in the Poisson–Voronoi case.

2 Some preliminaries

In the following we briefly introduce some mathematical notions and the basic notation used in this paper. Particularly, we emphasize the notion of stationary random tessellations and their typical cells in the d–dimensional Euclidean space $\mathbb{R}^d$, where we focus on the planar case $d = 2$. For a more detailed discussion of the mathematical background, especially in the case $d > 2$, it is referred to the literature, for example Schneider and Weil [11], and Stoyan, Kendall and Mecke [14]. Further information on random tessellations in $\mathbb{R}^d$ can also be found e.g. in Møller [9], and in Okabe et al. [10].

Consider the 2–dimensional Euclidean plane $\mathbb{R}^2$ with the Borel σ–algebra $\mathcal{B}(\mathbb{R}^2)$. For an arbitrary set $B \subset \mathbb{R}^2$, let $\operatorname{int} B, \partial B$, and B^c denote the interior, the boundary, and the complement, respectively. Furthermore, for any $B \in \mathcal{B}(\mathbb{R}^2)$, let $\nu_2(B)$ denote the 2–dimensional Lebesgue measure and let $b(o,1)$ be the unit ball with $\nu_2(b(o,1)) = \pi$. The families of all closed sets, compact sets, and convex bodies (compact and convex sets) in $\mathbb{R}^2$ are denoted by $\mathcal{F}$, $\mathcal{K}$, and $\mathcal{C}$, respectively.

Random closed sets and point processes A *random closed set* Ξ in $\mathbb{R}^2$ is a measurable mapping $\Xi : \Omega \to \mathcal{F}$ from some probability space $(\Omega, \sigma(\Omega), \mathbb{P})$ into the space $(\mathcal{F}, \mathcal{B}(\mathcal{F}))$, where $\mathcal{B}(\mathcal{F})$ denotes the smallest σ–algebra of subsets of $\mathcal{F}$ that contains all sets $\{F \in \mathcal{F}, F \cap K \neq \emptyset\}$ for any $K \in \mathcal{K}$. Particularly, Ξ is called a random compact set or a random convex body if $\mathbb{P}(\Xi \in \mathcal{K}) = 1$ or $\mathbb{P}(\Xi \in \mathcal{C}) = 1$, respectively. A random closed set Ξ is called *stationary* if its distribution is invariant under arbitrary translations in $\mathbb{R}^2$. Analogously, Ξ is called *isotropic* if its distribution is invariant under arbitrary rotations about the origin o, respectively.

Furthermore, the following notion of a point process of random closed sets is useful. A measurable mapping $X : \Omega \to N(\mathcal{F}')$ from some probability space $(\Omega, \sigma(\Omega), \mathbb{P})$ into the space $(N(\mathcal{F}'), \mathcal{N}(\mathcal{F}'))$ is called a *point process* in $\mathcal{F}'$, where $N(\mathcal{F}')$ denotes the family of all locally finite counting measures on $\mathcal{B}(\mathcal{F}')$ with $\mathcal{F}' = \mathcal{F} \setminus \{\emptyset\}$ and where $\mathcal{N}(\mathcal{F}')$ is the smallest σ–algebra of subsets of $N(\mathcal{F}')$ that contains all sets $\{\eta \in N(\mathcal{F}'), \eta(F \in \mathcal{F}', F \cap K \neq \emptyset) = k\}$ for any $k = 0, 1, \ldots$ and $K \in \mathcal{K}$. Stationarity and isotropy of X can be defined as in the case of random closed sets mentioned above. The mapping $\Lambda : \mathcal{B}(\mathcal{F}') \to [0, \infty]$ with $\Lambda(B) = \mathbb{E}(X(B))$ for any $B \in \mathcal{B}(\mathcal{F}')$ is called the *intensity measure* of X.

A *Poisson point process* X in $\mathcal{F}'$ is defined by two properties. First, the number of points $X(B)$ of X in a set $B \in \mathcal{B}(\mathcal{F}')$ with $\Lambda(B) < \infty$ is Poisson distributed with parameter $\Lambda(B)$ and, second, for arbitrary $n \geq 2$ and for any pairwise disjoint Borel sets $B_1, \ldots, B_n \in \mathcal{B}(\mathcal{F}')$ with $\Lambda(B_1) < \infty, \ldots, \Lambda(B_n) < \infty$, the random variables $X(B_1), \ldots, X(B_n)$ are independent.

Often it is sufficient to consider *simple* point processes, which means that there exists a sequence $(\Xi_n)_{n \in \mathbb{N}}$ of random closed sets $\Xi_n : \Omega \to \mathcal{F}'$ such that $X = \sum_{n=1}^{X(\mathcal{F}')} \delta_{\Xi_n}$ and $\Xi_n \neq \Xi_{n'}$ if $n \neq n'$. An important special case of a (simple) point process in $\mathcal{F}'$ is given if the random closed sets Ξ_n consist of single points only. Then, X is called a point process in $\mathbb{R}^2$ and can be considered as random counting measure on $\mathcal{B}(\mathbb{R}^2)$. Furthermore, in case of stationarity, there exists a constant $\lambda \geq 0$ (called the *intensity* of X) such that $\Lambda(B) = \lambda \nu_2(B)$ for any $B \in \mathcal{B}(\mathbb{R}^2)$.

Poisson line processes Consider the space $\mathcal{S}$ of all affine 1–dimensional subspaces in $\mathbb{R}^2$ and let $\mathcal{L} = \{L \in \mathcal{S} : o \in L\}$. A point process X in $\mathcal{F}'$ is called a (planar) *line process* if for the intensity measure Λ of X it holds that $\Lambda(\mathcal{F}' \setminus \mathcal{S}) = 0$. In case of stationarity, Λ can be disintegrated as follows.

Suppose that Λ is locally finite and not equal to the zero measure. Then, there exists a constant $\lambda_\ell \in (0,\infty)$ and a probability measure Θ on $\mathcal{B}(\mathcal{L})$, called the *orientation distribution* of X, such that

$$\Lambda(B) = \lambda_\ell \int_{\mathcal{L}} \int_{L^\perp} \mathbb{1}_B(L+x)\nu_1(dx)\Theta(dL) \tag{1}$$

for any $B \in \mathcal{B}(\mathcal{S})$, where ν_1 denotes the 1–dimensional Lebesgue–measure on the orthogonal complement $L^\perp \in \mathcal{L}$ of $L \in \mathcal{L}$. Notice that formula (1) yields that

$$\lambda_\ell = \frac{1}{2}\,\mathbb{E}X(L \in \mathcal{S} : L \cap b(o,1) \neq \emptyset)\,, \tag{2}$$

i.e., $2\lambda_\ell$ is the expected number of lines hitting $b(o,1)$. In particular, we consider the case that X is a stationary and isotropic Poisson line process. Then, Θ is the uniform distribution on $\mathcal{B}(\mathcal{L})$ and X can be represented in the form $X = \sum_{n\geq 1} \delta_{\ell_{(R_n,V_n)}}$, where $\{R_n\}$ is a stationary Poisson point process in $\mathbb{R}$ with intensity λ_ℓ and $\{V_n\}$ is an independent sequence of independent and identically distributed random variables with uniform distribution on $[0,\pi)$. For each line $\ell_{(R_n,V_n)}$, the angle V_n is measured in anti–clockwise direction between the x–axis and the outer orientation vector of the line, whereas R_n denotes the signed perpendicular distance of the line to the origin. Notice that Formula (1) can be written as

$$\Lambda(B) = \frac{\lambda_\ell}{\pi} \int_0^\pi \int_{\mathbf{R}} \mathbb{1}_B(\ell_{(r,v)})drdv\,, \qquad B \in \mathcal{B}(\mathcal{S})\,. \tag{3}$$

Furthermore, each line $\ell_{(R_n,V_n)}$ in $\mathbb{R}^2$ can be described by its Hessian normal form $\ell_{(R_n,V_n)} = \{(x,y) \in \mathbb{R}^2 : x\cos V_n + y \sin V_n = R_n\}$. It is easy to see that the expected total length $\mathbb{E}\sum_{n\geq 1} \nu_1(\ell_{(R_n,V_n)} \cap b(o,1))$ of lines $\ell_{(R_n,V_n)}$ in the unit ball $b(o,1)$ is given by $\pi\lambda_\ell$. Thus, $\gamma = \lambda_\ell$ is the expected total length per unit area and, therefore, called the *intensity* of the random closed set $X_\ell = \bigcup_{n\geq 1} \ell_{(R_n,V_n)}$. For simplicity, both X_ℓ and $X = \sum_{n\geq 1} \delta_{\ell_{(R_n,V_n)}}$ are called Poisson line processes in the following; see also Fig. 1a.

Cox processes induced by Poisson line processes In order to describe (doubly stochastic) point processes in $\mathbb{R}^2$ located on the lines of Poisson line processes, we use the concept of *Cox processes*, which can be seen as a generalization of (inhomogeneous) Poisson point processes in $\mathbb{R}^2$. More formally, let X_ℓ be a stationary and isotropic Poisson line process with intensity γ. Then, given X_ℓ, the Cox process X_c is a Poisson point process in $\mathbb{R}^2$ with (conditional) intensity measure $\Lambda_c(\cdot \mid X_\ell) = \lambda\nu_1(X_\ell \cap \cdot)$ for some $\lambda > 0$. In particular, X_c is a stationary and isotropic point process in $\mathbb{R}^2$ whose intensity measure Λ_c satisfies the relationships $\Lambda_c(\cdot) = \mathbb{E}X_c(\cdot) = \lambda\mathbb{E}\nu_1(X_\ell \cap \cdot) = \lambda\gamma\nu_2(\cdot)$, i.e., $\lambda_c = \lambda\gamma$ is the intensity of X_c. Furthermore, the point processes on the individual lines of the Poisson line process X_ℓ are (1–dimensional) Poisson point processes with intensity λ. Thus, λ can be interpreted as mean number of points per unit length of X_ℓ. In Fig. 1b, a realization of a Cox process is shown induced by Poisson point processes on the lines of a Poisson line process.

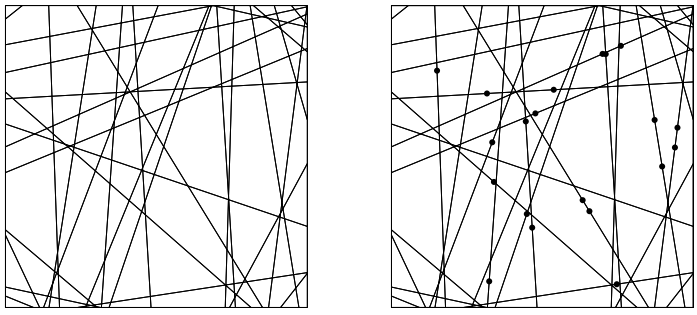

(a) Realization of a Poisson line process

(b) Realization of Cox points on the lines of a Poisson line process

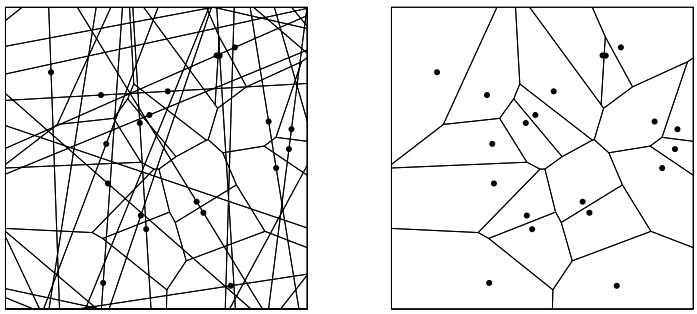

(c) Voronoi cells having Cox points as nuclei

(d) Realization of a Cox–Voronoi tessellation

Figure 1 Construction principle for the Cox–Voronoi tessellation ($\gamma = 0.1$ and $\lambda = 0.04$)

Random tessellations A *tessellation* in $\mathbb{R}^2$ is some countable family $\tau = \{C_n\}_{n\geq 1}$ of convex bodies $C_n \in \mathcal{C}$ such that $\operatorname{int} C_n \neq \emptyset$ for all n, $\operatorname{int} C_n \cap \operatorname{int} C_m = \emptyset$ for all $n \neq m$, $\bigcup_{n\geq 1} C_n = \mathbb{R}^2$, and $\sum_{n\geq 1} \mathbb{1}_{\{C_n \cap K \neq \emptyset\}} < \infty$ for any $K \in \mathcal{K}$. Notice that the sets C_n, called the *cells* of τ, are polytopes in $\mathbb{R}^2$. The family of all tessellations in $\mathbb{R}^2$ is denoted by $\mathcal{T}$. A *random tessellation* in $\mathbb{R}^2$ is a (simple) point process $\sum_{n\geq 1} \delta_{\Xi_n}$ in $\mathcal{F}'$ such that $\mathbb{P}(\{\Xi_n\}_{n\geq 1} \in \mathcal{T}) = 1$. Notice that a random tessellation can also be considered as a marked point process $X_\tau = \sum_{n\geq 1} \delta_{[\alpha(\Xi_n), \Xi_n^0]}$ in $\mathbb{R}^2$, where $\alpha : \mathcal{C}' \to \mathbb{R}^2$, $\mathcal{C}' = \mathcal{C}\backslash\{\emptyset\}$, is a measurable mapping such that $\alpha(C) \in C$ and $\alpha(C + x) = \alpha(C) + x$ for any $C \in \mathcal{C}'$ and $x \in \mathbb{R}^d$, and where $\Xi_n^0 = \Xi_n - \alpha(\Xi_n)$ is the centered cell corresponding to Ξ_n which contains the origin. The point $\alpha(C) \in \mathbb{R}^2$ is called an *associated point* of C and can be chosen, for example, to be the lexicographically smallest point of C.

It is not difficult to see that the lines of a stationary and isotropic Poisson line process X_ℓ induce a (stationary and isotropic) random tessellation in $\mathbb{R}^2$, which is called a *Poisson line tessellation* (PLT); see Fig. 2a. Furthermore, for any point process $X = \sum_{n\geq 1} \delta_{P_n}$ in $\mathbb{R}^2$, consider the

random sets $\Xi_n = \{x \in \mathbb{R}^2 : |x - P_n| \leq |x - P_m| \text{ for and } m \neq n\}$. If $\mathbb{P}(\{\Xi_n\}_{n\geq 1} \in \mathcal{T}) = 1$, then $X_\tau = \sum_{n\geq 1} \delta_{\Xi_n}$ is called a *Voronoi tessellation* induced by X, where P_n is called the *nucleus* of Ξ_n. Notice that the nuclei of Voronoi tessellations can be considered as associated points of their cells. In particular, X_τ is called a *Poisson–Voronoi tessellation* (PVT) if X is a Poisson process; see Fig. 2b. Similarly, X_τ is called a *Cox–Voronoi tessellation* (CVT) if X is a Cox process; see Fig. 1c,d. Furthermore, the triangulation, which arises when the nuclei of neighboring cells of a PVT are connected, is called a *Poisson–Delaunay tessellation* (PDT); see Fig. 2c.

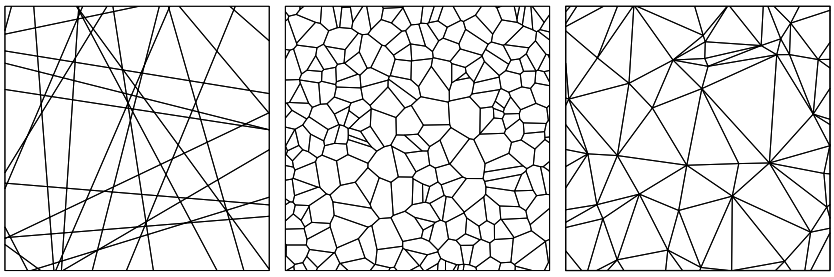

(a) PLT (b) PVT (c) PDT

Figure 2 Realizations of three basic tessellation models: PLT, PVT, PDT

Typical cell and zero cell of stationary tessellations Suppose that the marked point process $X_\tau = \sum_{n\geq 1} \delta_{[\alpha(\Xi_n),\Xi_n^0]}$ is stationary with positive and finite intensity $\lambda_\tau = \mathbb{E}\#\{n : \alpha(\Xi_n) \in [0,1)^2\}$. By $\mathcal{P}^0$ we denote the family of all convex polytopes with their associated point at the origin. Then, the *Palm mark distribution* P^0 of X_τ is given by $P^0(B) = \lambda_\tau^{-1}\,\mathbb{E}\#\{n : \alpha(\Xi_n) \in [0,1)^2,\, \Xi_n^0 \in B\}$ for any $B \in \mathcal{B}(\mathcal{F}) \cap \mathcal{P}^0$. Notice that a random polytope $\Xi^* : \Omega \to \mathcal{P}^0$, whose distribution coincides with P^0, is called the *typical cell* of X_τ. Furthermore, it holds that

$$\lambda_\tau^{-1} = \int_{\mathcal{P}^0} \nu_2(C)\, P^0(dC)\,, \tag{4}$$

i.e., the expected area $\mathbb{E}\nu_2(\Xi^*) = \int_{\mathcal{P}^0} \nu_2(C)\, P^0(dC)$ of the typical cell Ξ^* is equal to λ_τ^{-1}.

The zero cell Ξ^0 of a stationary tessellation X_τ is defined to be the cell which contains the origin o, i.e., $\Xi^0 = \Xi_n$ if $o \in \operatorname{int} \Xi_n$. Up to translation, the distribution of the zero cell (of stationary tessellations) is the area–weighted distribution of the typical cell. In particular, for any translation–invariant, non–negative and measurable functional $f : \mathcal{C} \to \mathbb{R}$ we have that

$$\mathbb{E}f(\Xi^0) = \lambda_\tau \mathbb{E}(f(\Xi^*)\,\nu_2(\Xi^*))\,. \tag{5}$$

Moreover, it holds that $\mathbb{P}(\nu_2(\Xi^0) \leq x) \leq \mathbb{P}(\nu_2(\Xi^*) \leq x)$ for any $x \geq 0$. This immediately implies that $\mathbb{E}\nu_2^k(\Xi^0) \geq \mathbb{E}\nu_2^k(\Xi^*)$ for each $k = 1, 2, \ldots$.

3 Typical cell of stationary CVT

A simulation algorithm, based on Slivniak's theorem concerning the Palm distribution of stationary point processes of Poisson type (see e.g. [11], [14]) is given for the typical cell of stationary CVT. See also [6] for algorithms to simulate the typical cell of other stationary tessellations.

Representation of the typical cell The typical cell Ξ^* of a CVT X_τ can be given as follows. Assume that the Cox process X_c of nuclei has intensity $\lambda_c = \lambda\gamma$ and is induced by a Poisson line process X_ℓ with intensity γ as described in Section 2. Let $\ell_{(o,V_0')}$ be a line through the origin with orientation angle V_0' which is independent of X_c and uniformly distributed on $[0, 2\pi)$. Furthermore, given V_0', let X^* be an independent stationary Poisson point process on $\ell_{(o,V_0')}$ with intensity λ. Then, by Slivniak's theorem, the typical cell Ξ^* of X_τ has the same distribution as the zero cell of the Voronoi tessellation induced by the superimposed point process $X_c + X^* + \delta_o$.

Simulation algorithm To simulate the Poisson line process X_ℓ radially, i.e., with increasing distance from the origin, it is sufficient to simulate independent random variables $T_i \sim \mathsf{Exp}(2\gamma)$ and $V_i' \sim \mathsf{U}[0, 2\pi]$ for each $i \in \{1, \ldots, k\}$ and for some $k \geq 1$. Then, k simulated lines can be obtained from the pairs (R_i', V_i'), where $R_i' = \sum_{j=1}^{i} T_j$. In view of this and because of the representation of the typical cell Ξ^* mentioned above, our algorithm, visualized in Fig. 3, starts by simulating the initial line $\ell_1 = \ell_{(o,V_0')}$ through the origin o with uniform orientation on $[0, 2\pi)$. The nearest–neighbor points P_1 and P_2 in each direction of ℓ_1 then have Euclidean distances Y_1 and Y_2 from o, where Y_1 and Y_2 are independent and $\mathsf{Exp}(\lambda)$–distributed; see Figure 3a.

Afterwards a uniformly oriented second line $\ell_2 = \ell_{R_1', V_1'}$ is simulated, where $R_1' \sim \mathsf{Exp}(2\gamma)$, and the point of intersection P_{ℓ_1,ℓ_2} between ℓ_1 and ℓ_2 is computed. Then, the nearest–neighbor points of P_{ℓ_1,ℓ_2}, say P_3 and P_4, are simulated on ℓ_2 using the memoryless property of the one–dimensional Poisson process on ℓ_2, i.e., the distances of the nearest–neighbor points in each direction of ℓ_2 from the point of intersection P_{ℓ_1,ℓ_2} are again $\mathsf{Exp}(\lambda)$–distributed; see Figure 3b. The four points P_1, P_2, P_3, and P_4, together with the origin o, are used to construct a first initial cell by computing the Voronoi cell of o with respect to the set $\{o, P_1, P_2, P_3, P_4\}$. Notice that by using the general construction principle of Voronoi tessellations, this initial cell provides an upper bound for the maximum distance from o to all those lines of X_ℓ that can influence the shape of the Voronoi cell with o as its nucleus.

This maximum distance equals two times the maximum distance of all vertices of the initial cell from o; see Fig. 3c. Notice that for simulating

the typical Cox–Voronoi cell it is not necessary to simulate further points on ℓ_1, since they can not influence the typical cell. This is due to the fact that all bisectors of points on ℓ_1 with respect to o are parallel to each other and hence have no point of intersection. For ℓ_2 this is not the case, meaning that further points have to be simulated with an exponentially distributed distance to the adjacent point on ℓ_2. By simulating further lines $\ell_{i+1} = \ell_{(R'_i, V'_i)}, i \geq 2$ with $R'_{i-1} < R'_i$ and $R'_i - R'_{i-1} \sim \mathsf{Exp}(2\gamma)$, and by simulating appropriately many points on these lines, it is finally possible to generate a cell whose distribution coincides with the distribution of the typical cell; see Fig. 3d.

For the purpose of short run–times, it is advisable to adjust the new maximum distance after having simulated a new line with simulated points on it and after having constructed the corresponding bisectors with regard to o. This means if the considered cell is split by a bisector of one of the newly simulated points, it is possible that the regarded maximum distance can be reduced. The whole procedure is carried out until the distance of the next simulated line from o is bigger than the maximum distance, which is equal to two times the maximum distance from all vertices of the regarded cell to o.

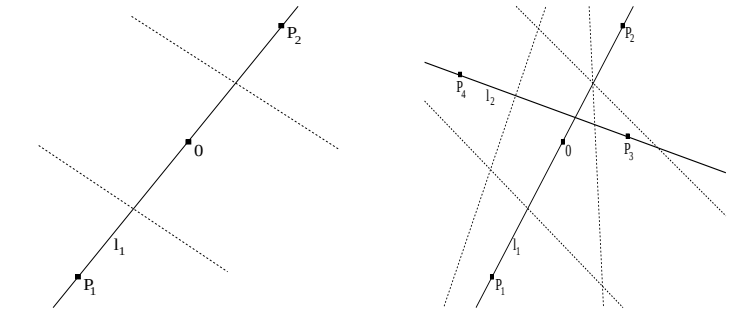

(a) *Initial line ℓ_1 with points o, P_1 and P_2* (b) *Second line ℓ_2 with points P_3 and P_4*

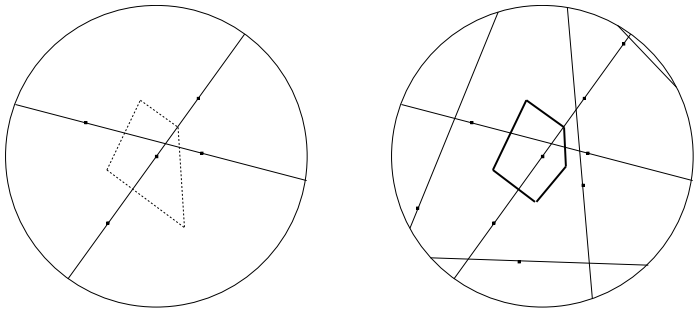

(c) *Initial cell* (d) *Typical cell*

Figure 3 *Simulation algorithm for the typical Cox–Voronoi cell*

4 Algorithm tests

Of course, the implementation of an algorithm has to be tested in order to detect implementation errors. In the present paper, three different types of statistical tests are applied in order to evaluate the simulation algorithm described in Section 3, where different (known) properties of the typical cell are used. Firstly, we use the fact that the mean area of the typical cell is reciprocal to the intensity (in our case $\lambda_c = \gamma\lambda$) of the corresponding tessellation; see (4). Secondly, applying the relationship (5) between functionals of the zero cell and of the typical cell, we get estimates for characteristics of the zero cell by simulating the typical cell and compare them to results directly obtained by simulation of the zero cell. Finally, we use a certain scaling property, i.e. the fact that the expectations of certain (appropriately scaled) characteristics of CVT do not depend on the quotient γ/λ. In this way, it is possible to test the algorithm by running it for different values of the input parameters λ and γ such that γ/λ is fixed.

Area test In order to analyze the expected area $\mathbb{E}\nu_2(\Xi^*)$ of the typical cell Ξ^* of a CVT X_τ, recall that (4) holds, i.e., $\mathbb{E}\nu_2(\Xi^*) = (\lambda\gamma)^{-1}$, where γ is the intensity of the Poisson line process X_ℓ and λ is the mean number of points per unit length of X_ℓ. Therefore it is reasonable to test the null-hypothesis that the expectation of results for the area of the typical cell Ξ^* provided by the implemented algorithm should be equal to $(\lambda\gamma)^{-1}$. To evaluate such a null–hypothesis a well–known statistical test is used, where $n = 2000000$ realizations $\tilde{\xi}_1^*, \ldots, \tilde{\xi}_n^*$ of the implemented version $\tilde{\Xi}^*$ of the typical cell Ξ^* were generated to get the estimate $\frac{1}{n}\sum_{i=1}^n \tilde{\nu}_2(\tilde{\xi}_i^*)$ for $\mathbb{E}\nu_2(\Xi^*)$, where $\tilde{\nu}_2(\tilde{\xi}_i^*)$ denotes the result for the area of a realization $\tilde{\xi}_i$ provided by the implementation of the algorithm. Since the underlying sampling variables $\tilde{\nu}_2(\tilde{\Xi}_i^*)$ are supposed to be independent and identically distributed and since our sample size n is large enough, the test statistic

$$T = \sqrt{n}\,\frac{\frac{1}{n}\sum_{i=1}^n \tilde{\nu}_2(\tilde{\Xi}_i^*) - (\lambda\gamma)^{-1}}{\sqrt{\frac{1}{n-1}\sum_{i=1}^n \left(\tilde{\nu}_2(\tilde{\Xi}_i^*) - \frac{1}{n}\sum_{i=1}^n \tilde{\nu}_2(\tilde{\Xi}_i^*)\right)^2}}$$

is nearly $\mathrm{N}(0,1)$–distributed; see e.g. [3]. Thus, an asymptotic Gaussian test can be applied to get inference about the null–hypothesis. Table 1 shows the p–values of such test for different values of γ and $c = \gamma/\lambda$, where for a significance level of $\alpha = 0.05$, say, the null–hypothesis is rejected only once for all regarded cases, which coincides well with the definition of the significance level. As conclusion, it can be assumed that the algorithm provides correct values for the expected area of the typical Cox–Voronoi cell.

Tests using comparison with the zero cell By (5), a second possibility to test the correctness of the algorithm can be provided. Given an implementation to simulate the zero cell Ξ^0 of X_τ, estimated characteristics

Table 1 Area tests for the typical Cox–Voronoi cell algorithm: p–values

γ	0.125	0.25	0.4	0.5	0.8	1.0	1.25	1.5
c=10	0.994	0.608	0.972	0.675	0.958	0.979	0.582	0.158
c=50	0.778	0.693	0.932	0.917	0.082	0.114	0.002	0.798
c=120	0.092	0.745	0.760	0.434	0.436	0.880	0.347	0306

Table 2 Tests by comparison with zero cell algorithm (fixed c): p–values

(a) $c = 10$

γ	η	ν_1	ν_2
0.125	0.067	0.068	0.139
0.25	0.187	0.308	0.237
0.4	0.104	0.020	0.057
0.5	0.391	0.536	0.780
0.8	0.174	0.377	0.255
1.0	0.108	0.019	0.033
1.25	0.696	0.632	0.673
1.5	0.805	0.508	0.431

(b) $c = 120$

γ	η	ν_1	ν_2
0.125	0.741	0.827	0.759
0.25	0.284	0.080	0.057
0.4	0.335	0.157	0.160
0.5	0.652	0.632	0.758
0.8	0.673	0.749	0.829
1.0	0.285	0.178	0.232
1.25	0.471	0.509	0.387
1.5	0.637	0.756	0.793

$\hat{\eta}(\hat{\Xi}^0)$, $\hat{\nu}_1(\hat{\partial}\hat{\Xi}^0)$ and $\hat{\nu}_2(\hat{\Xi}^0)$ for the number of vertices $\eta(\Xi^0)$, the perimeter $\nu_1(\partial\Xi^0)$, and the area $\nu_2(\Xi^0)$, respectively; are compared to estimated area–weighted characteristics of the typical Cox–Voronoi cell Ξ^*, where the latter are computed by using our algorithm to be tested. Then, similar to the situation of the area test described above, we arrive at (asymptotic Gaussian) two–sample tests for the equality of two expectations. Here 2000000 realizations of $\tilde{\Xi}^*$ and 2000000 realizations of $\hat{\Xi}^0$ were generated to verify null–hypotheses, stating that

- $\mathbb{E}\hat{\eta}(\hat{\Xi}^0) = \lambda\gamma\,\mathbb{E}(\tilde{\eta}(\tilde{\Xi}^*)\,\tilde{\nu}_2(\tilde{\Xi}^*))$
- $\mathbb{E}\hat{\nu}_1(\hat{\partial}\hat{\Xi}^0) = \lambda\gamma\,\mathbb{E}(\tilde{\nu}_1(\tilde{\partial}\tilde{\Xi}^*)\,\tilde{\nu}_2(\tilde{\Xi}^*))$
- $\mathbb{E}\hat{\nu}_2(\hat{\Xi}^0) = \lambda\gamma\,\mathbb{E}\tilde{\nu}_2^2(\tilde{\Xi}^*)$.

Table 2 depicts resulting p–values for fixed values of $c = \gamma/\lambda$ and different values of γ, while Table 3 lists p–values for fixed γ but varying c. These tables show that regarding a significance level of $\alpha = 0.05$, the number of cases where the null–hypothesis is actually rejected is very close to the theoretically expected number under the null–hypothesis. Therefore the comparison between our algorithm for the typical Cox–Voronoi cell and a zero cell algorithm assures that our algorithm provides correct estimates, assuming that the algorithm for the zero cell is correct.

Tests using invariance properties under scaling Notice that a certain zooming effect can be observed for the CVT introduced in Section 2. More precisely, for $c = \gamma/\lambda$ fixed, the following scaling–invariance properties hold. Suppose that $\gamma = a\gamma_0$ and $\lambda = a\lambda_0$ for some $\gamma_0, \lambda_0 > 0$ fixed and $a \to 0$.

Table 3 Tests by comparison with zero cell algorithm ($\gamma = 0.125$): p–values

c	η	ν_1	ν_2
20	0.653	0.704	0.705
30	0.859	0.608	0.642
40	0.733	0.770	0.783
60	0.424	0.700	0.636
90	0.316	0.187	0.210

Then, the expected number of vertices of the typical cell is constant, whereas the expected perimeter and the square root of the expected area of the typical cell grow linearly, proportionally to a^{-1}. As a conclusion, it is possible to test the equality of (suitably scaled) expectations for results provided by the implementation of the algorithm for a fixed value of c and for different values of γ and λ, respectively. Moreover, similar scaling properties are true for higher–order moments of the number of vertices, the perimeter and the expected area of the typical cell. Thus, after suitable scaling, testing the equality of variances is also possible. For different values of the pair (γ, λ) with a constant quotient $c = \gamma/\lambda$, 2000000 realizations of $\tilde{\Xi}^*$ were generated and estimates of (suitably scaled) expectations of the number of vertices, the perimeter and the expected area of the typical cell were computed. Using the same type of (asymptotic Gaussian) two–sample tests as in the case described above, the equality of these expectations provided by the algorithm can be verified. Regarding the equality of the estimation for the expected perimeters provided by the implementation, the p–values are displayed in Table 4 for $c = 50$. Furthermore, 2000000 realizations of $\tilde{\Xi}^*$ were generated for each of 3 different values of $c = \gamma/\lambda$ and 8 different values of γ, where asymptotic Levene–type tests have been performed for the null-hypothesis of equality of 8 variances of the number of vertices as well as of (suitably scaled) perimeter and area of the typical cell, respectively. Notice once more, that always the equality of expectations for the estimates provided by the implementation of the algorithm are tested, not the equality of expectations for theoretical characteristics. Here the quantiles of the (asymptotic) χ^2_7–distribution of the test statistics are used to compute the p–values for the 3 considered values of c. They are displayed in Table 5. For other choices of c and γ, we obtained similar results, which justifies to state that the algorithm behaves as expected.

5 Numerical results

In this section, some numerical results for the typical Cox–Voronoi cell Ξ^* are presented, which have been obtained by the simulation algorithm described in Section 3. Of particular interest are distributional properties as well as first–order and second–order moments of cell characteristics such as area, perimeter, and number of vertices. Apart from that, differences to the

Table 4 Tests for equality of expected perimeter estimates ($c = 50$): p–values

γ/γ	0.125	0.25	0.4	0.5	0.8	1.0	1.25	1.5
0.125	–	0.636	0.373	0.393	0.918	0.928	0.995	0.437
0.25	0.636	–	0.251	0.268	0.851	0.867	0.986	0.306
0.4	0.373	0.251	–	0.521	0.957	0.963	0.998	0.566
0.5	0.3933	0.268	0.521	–	0.951	0.958	0.998	0.544
0.8	0.918	0.851	0.957	0.951	–	0.527	0.878	0.061
1.0	0.928	0.86679	0.962	0.958	0.527	–	0.863	0.053
1.25	0.995	0.986	0.998	0.998	0.878	0.863	–	0.003
1.5	0.437	0.306	0.566	0.544	0.061	0.053	0.003	–

Table 5 Levene's test for equality of variances: p–values

c	η	ν_1	ν_2
10	0.457	0.883	0.907
50	0.034	0.623	0.296
120	0.449	0.608	0.603

behavior of corresponding characteristics of the typical cell of classical PVT are examined.

Distributional properties For all simulations we used $n = 2000000$ iterations. In Figure 4 histograms for the area, the number of vertices, and the perimeter of the typical Cox–Voronoi cell are displayed, where $\gamma = 0.125$ and $c = 60$ or $c = 90$, respectively. At first sight, the area seems to follow a Gamma–distribution, whereas the histogram for the perimeter of the typical cell looks like a histogram of a normal distribution. Furthermore, the histograms of the number of vertices seem to have similar shape as the one for the area, but this time in a discrete version. Notice also that the modes of the latter two histograms coincide with the expectation $\mathbb{E}\eta(\Xi^*) = 6$ of the underlying theoretical distributions. For other choices of parameters c and γ, the histograms look quite similar.

First–order and second–order moments Table 6 shows simulation results for functionals $f(\Xi^*)$ of the typical Cox–Voronoi cell Ξ^*, where $f(\Xi^*)$ is either $\nu_2(\Xi^*)$ (area), $\nu_1(\partial\Xi^*)$ (perimeter), or $\eta(\Xi^*)$ (number of vertices).

Besides the expectations $\mathbb{E}f(\Xi^*)$, the variances $\mathrm{Var}f(\Xi^*)$ as well as the coefficients of variation $\mathrm{cv}f(\Xi^*) = 100\sqrt{\mathrm{Var}f(\Xi^*)}/\mathbb{E}f(\Xi^*)$ (i.e., standard deviation times 100 divided by expectation) are also displayed in Table 6, where results are shown for different values of γ and fixed parameter $c = \gamma/\lambda = 50$. Recall that in the case presented in Table 6, i.e. for different values of γ and fixed c, the moments $\mathbb{E}f(\Xi^*)$ and $\mathrm{Var}f(\Xi^*)$, respectively, are related to each other by scaling. For example, $\mathbb{E}\eta(\Xi^*)$ does not depend on γ, whereas $\mathbb{E}\nu_1(\partial\Xi^*)$ and $\sqrt{\mathbb{E}\nu_2(\Xi^*)}$ are linear with respect to $1/\gamma$. These scaling properties are nicely reflected by the simulated estimates given in

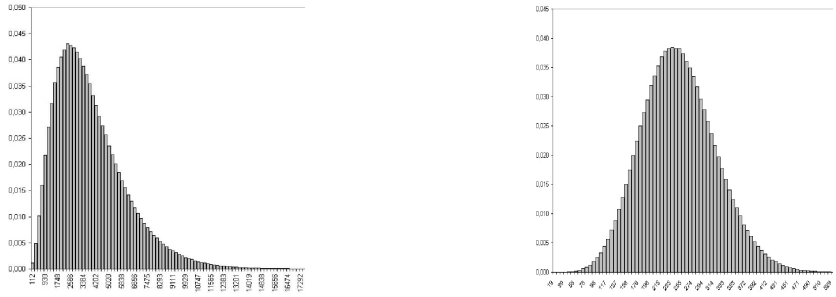

(a) Area (b) Perimeter

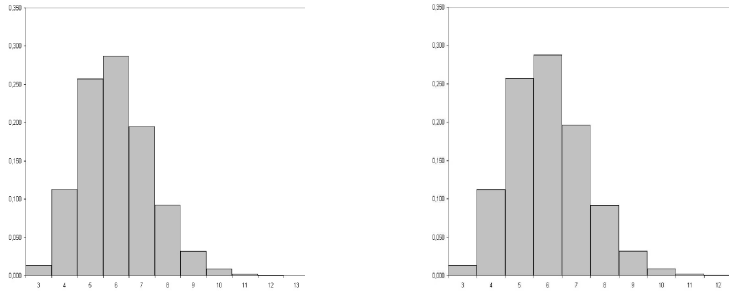

(c) Number of vertices ($c = 60$) (d) Number of vertices ($c = 90$)

Figure 4 Histograms for characteristics of the typical Cox–Voronoi cell

Table 6. In particular, the coefficients of variation given in Table 6 show that similar scaling properties, analogous to those for expectations, hold with respect to variances.

In Table 7, the dual case is considered for some fixed γ and for different values of c. Furthermore, by the same scaling properties as mentioned above, the simulated estimates given in Table 7 can be used in order to compute estimates for $\mathbb{E}f(\Xi^*)$, $\mathrm{Var}f(\Xi^*)$, and $\mathrm{cv}f(\Xi^*)$ for any $c \in \{10, 20, 30, 40, 50, 60, 90, 120\}$ and γ arbitrary. For example, for $c = 20$ and $\gamma = 0.25$, we would get the estimates 6.001, 71.136, and 320.073 for $\mathbb{E}\eta(\Xi^*)$, $\mathbb{E}\nu_1(\partial\Xi^*)$, and $\mathbb{E}\nu_2(\Xi^*)$, respectively. If we would like to know estimates for some $c \notin \{10, 20, 30, 40, 50, 60, 90, 120\}$, they could either be determined by interpolation from the data given in Table 7, or by simulation for the value of c under consideration and for some fixed γ and, afterwards, for the desired values of γ by using the scaling properties. Moreover, looking at the estimates for $\mathbb{E}\eta(\Xi^*)$ given in Table 7, we see that all these estimates are almost equal to 6 for any c, which is conform with the scaling invariance of $\mathbb{E}\eta(\Xi^*)$. However, the estimates for the variances $\mathrm{Var}\eta(\Xi^*)$ seem to slightly decrease for increasing c. On the other hand, the estimates for expectations and variances of perimeter and area, respectively, increase for

Table 6 Estimates for first–order and second–order moments for $c = 50$ and different values of γ

	γ	$\mathbb{E}f(\Xi^*)$	$\mathrm{Var}f(\Xi^*)$	$\mathrm{cv}f(\Xi^*)$
$\eta(\Xi^*)$	0.125	6.000	1.892	22.925
	0.25	6.001	1.896	22.945
	0.4	5.998	1.896	22.957
	0.5	5.999	1.897	22.959
	0.8	6.000	1.895	22.943
	1.0	6.001	1.896	22.945
	1.25	6.001	1.900	22.970
	1.5	6.001	1.900	22.970
$\nu_1(\partial\Xi^*)$	0.125	225.207	3912.919	27.776
	0.25	112.617	976.756	27.752
	0.4	70.370	382.203	27.782
	0.5	56.297	244.286	27.763
	0.8	35.205	95.521	27.762
	1.0	28.165	61.139	27.762
	1.25	22.540	39.168	27.766
	1.5	18.766	27.134	27.758
$\nu_2(\Xi^*)$	0.125	3198.954	3747622.689	60.516
	0.25	799.828	233774.327	60.451
	0.4	312.300	35711.831	60.511
	0.5	199.882	14625.775	60.504
	0.8	78.172	2234.666	60.472
	1.0	50.026	914.832	60.461
	1.25	32.040	375.760	60.501
	1.5	22.212	180.516	60.488

increasing c, whereas, interestingly enough, the estimates for the coefficients of variation decrease for increasing c.

Comparison to PVT Another interesting effect occurs when the expected perimeter $\mathbb{E}\nu_1(\partial\Xi^*)$ of the typical cell Ξ^* of a CVT is compared to the expected perimeter $\mathbb{E}\nu_1(\partial\Xi^*_{PVT})$ of the typical cell Ξ^*_{PVT} of a PVT with the same intensity. Notice that for the typical cell Ξ^*_{PVT} of a PVT with intensity λ_{PVT} it holds that

$$\mathbb{E}\nu_2(\Xi^*_{PVT}) = \frac{1}{\lambda_{PVT}}, \quad \mathbb{E}\nu_1(\partial\Xi^*_{PVT}) = \frac{4}{\sqrt{\lambda_{PVT}}}, \quad \mathbb{E}\eta(\Xi^*_{PVT}) = 6\,. \quad (1)$$

In particular, $\mathbb{E}\eta(\Xi^*_{PVT}) = \mathbb{E}\eta(\Xi^*)$ and, assuming that $\lambda_{PVT} = \lambda\gamma$, we have $\mathbb{E}\nu_2(\Xi^*_{PVT}) = \mathbb{E}\nu_2(\Xi^*)$. Furthermore, using the second formula in (1), we can compare the expected perimeter $\mathbb{E}\nu_1(\partial\Xi^*_{PVT})$ to the estimate for $\mathbb{E}\nu_1(\partial\Xi^*)$ obtained by the simulation algorithm described in Section 3. Some numerical results are displayed in Tables 8 and 9, where it is assumed that the expected areas $\mathbb{E}\nu_2(\Xi^*_{PVT})$ and $\mathbb{E}\nu_2(\Xi^*)$ coincide, being equal

Table 7 Estimates for first–order and second–order moments for $\gamma = 0.125$ and different values of c

	c	$\mathbb{E}f(\Xi^*)$	$\mathrm{Var}f(\Xi^*)$	$\mathrm{cv}f(\Xi^*)$
$\eta(\Xi^*)$	10	5.998	2.088	24.091
	20	6.001	1.981	23.454
	30	6.002	1.939	23.200
	40	6.002	1.915	23.056
	50	5.999	1.892	22.929
	60	6.000	1.883	22.870
	90	5.999	1.863	22.752
	120	6.000	1.850	22.669
$\nu_1(\partial\Xi^*)$	10	100.500	1000.239	31.469
	20	142.271	1771.053	29.580
	30	174.355	2501.238	28.684
	40	201.424	3210.422	28.130
	50	225.207	3912.919	27.776
	60	246.843	4599.240	27.474
	90	302.432	6640.160	26.944
	120	349.528	8637.773	26.590
$\nu_2(\Xi^*)$	10	639.216	197578.455	69.538
	20	1280.290	688685.388	64.819
	30	1920.488	1447118.677	62.638
	40	2560.610	2467092.919	61.340
	50	3198.953	3747622.689	60.516
	60	3840.243	5272317.126	59.792
	90	5758.732	11386016.845	58.595
	120	7684.181	19751363.890	57.836

Table 8 Expected perimeters of Ξ^*_{PVT} and Ξ^* provided that $\mathbb{E}\nu_2(\Xi^*_{PVT}) = \mathbb{E}\nu_2(\Xi^*) = 100$

c	γ	λ	λ_{PVT}	CVT	PVT
10	0.3162	0.03162	0.0100	39.731	40.000
20	0.4472	0.02237	0.0100	39.785	40.000
30	0.5477	0.01826	0.0100	39.793	40.000
40	0.6325	0.01581	0.0100	39.807	40.000
50	0.7071	0.01414	0.0100	39.832	40.000
60	0.77460	0.01291	0.0100	39.834	40.000
90	0.9487	0.01054	0.0100	39.848	40.000
120	1.095	0.00913	0.0100	39.879	40.000

Table 9 Expected perimeters of Ξ^*_{PVT} and Ξ^* provided that $\mathbb{E}\nu_2(\Xi^*_{PVT}) = \mathbb{E}\nu_2(\Xi^*) = 625$

c	γ	λ	λ_{PVT}	CVT	PVT
10	0.1265	0.01265	0.00160	99.312	100.000
20	0.1789	0.00895	0.00160	99.407	100.000
30	0.2191	0.00730	0.00160	99.472	100.000
40	0.2530	0.00633	0.00160	99.518	100.000
50	0.2828	0.00566	0.00160	99.593	100.000
60	0.3098	0.00516	0.00160	99.598	100.000
90	0.3795	0.00422	0.00160	99.615	100.000
120	0.4382	0.00365	0.00160	99.699	100.000

to 40 and 100, respectively. Similar results are obtained for other values of $1/\lambda_{PVT}$, where the following qualitative behavior is observed. The estimates for the expected perimeter of the typical Cox–Voronoi cell increase with increasing c but seem to be in any case smaller than the expected perimeter of the typical cell of a PVT with the same intensity. A possible explanation of this interesting behavior could be the fact that the typical cell of CVT is more regular than the typical cell of PVT, because two edges of the typical Cox–Voronoi cell can be parallel with some positive probability. In the case of a PVT this probability is equal to zero.

Acknowledgements This research was supported by France Télécom through research grant 42 36 68 97. The authors are grateful to Michael Rösch for his help in performing the large–scale simulations, which lead to the numerical results.

References

1. Binder RV (2000) *Testing Object-Oriented Systems: Models, Patterns and Tools*. Addison-Wesley, Boston.
2. Błaszczyszyn B and Schott R (2004) Approximations of functionals of some modulated–Poisson Voronoi tessellations with applications to modeling of communication networks. Preprint.
3. Casella C and Berger RL (2002) *Statistical Inference*. Wadsworth, Duxbury.
4. Gloaguen G, Coupé P, Maier R and Schmidt V (2002) Stochastic modelling of urban access networks. *Proceedings of IEEE Infocom '02*, München.
5. Gloaguen G, Fleischer F, Schmidt H and Schmidt V (2004) Fitting of stochastic telecommunication network models, via distance measures and Monte-Carlo tests. Preprint.
6. Maier R, Mayer J and Schmidt V (2004) Distributional properties of the typical cell of stationary iterated tessellations. *Mathematical Methods of Operations Research* 59:287–302.
7. Mayer J and Guderlei R (2004) Test oracles and randomness. *Lecture Notes in Informatics* P-58:179–189, Köllen Druck+Verlag GmbH, Bonn.

8. Mayer J, Schmidt V and Schweiggert F (2004) A unified simulation framework for spatial stochastic models. *Simulation Modelling Practice and Theory* 12:307–326.
9. Møller J (1989) Random tessellations in $\mathbb{R}^d$. *Advances in Applied Probability* 21:37–73.
10. Okabe A, Boots B, Sugihara K and Chiu SN (2000) *Spatial Tessellations*. 2nd ed., J.Wiley & Sons, Chichester.
11. Schneider R and Weil W (2000) *Stochastische Geometrie*. Teubner, Stuttgart.
12. Schütz GJ, Axmann M, Freudenthaler S, Schindler H, Kandror K, Roder JC and Jeromin A (2004) Visualization of vesicle transport along and between distinct pathways in neurites of living cells. *Microscopy Research and Technique* 63:159–167.
13. Sneed HM and Winter M (2002) *Testen objektorientierter Software*, 1st ed., Hanser, München.
14. Stoyan D, Kendall WS and Mecke J (1995) *Stochastic Geometry and its Applications*. 2nd ed., J. Wiley & Sons, Chichester.